

Microstructure and Mechanical Properties of Dissimilar TC4 Titanium Alloy/304 Stainless Steel Joint Using Copper Filler Wire



XIAOHU HAO, PENG LI, YUEQING XIA, HONGGANG DONG, PENGXIAO WANG,
and DEJUN YAN

TC4 titanium alloy was successfully welded to 304 stainless steel using gas tungsten arc welding with a CuSi3 filler wire. The Ti/weld transition zone in the joint consisted of β -Ti, Ti_2Cu , $AlCu_2Ti$, $TiCu$, and Ti_5Si_3 intermetallic compounds (IMCs) when welded with low current. As the welding current increased, more Fe dissolved into the weld pool, and massive ternary Ti-Cu-Fe and $AlCu_2Ti$ IMCs formed in the Ti/weld transition zone. The segregated Ti_5Si_3 phase disappeared, and complex Fe-Ti-Si-Cr IMCs formed outside the Ti/weld transition zone. The microhardness was much higher in the Ti/weld transition zone than that in the TC4 substrate and copper weld, reaching a maximum value of 619 HV. The highest tensile strength was 328 MPa when the welding current was 120 A and the traveling speed was 4 mm/s. All joints failed through the Ti/weld transition zone, and brittle cleavage features were present on the fractured surfaces. Due to the large difference in thermophysical properties between the two base metals, cracks were easily generated, which restricted the improvement in the tensile strength of the TC4/304 SS joint.

<https://doi.org/10.1007/s11661-018-5031-3>

© The Minerals, Metals & Materials Society and ASM International 2018

I. INTRODUCTION

A hybrid titanium and steel structure can combine the respective advantages of two materials, facilitating widespread applications in the aeronautics, astronautics, chemical, and nuclear industries.^[1,2] However, residual welding stress and brittle intermetallic compounds (IMCs) caused by the large mismatch of thermal–physical properties and metallurgical incompatibility usually degrade the mechanical properties of the resulting dissimilar joints.^[3,4] Various welding technologies, such as friction welding,^[5,6] explosive welding,^[7,8] hot-roll bonding,^[9,10] diffusion welding,^[11,12] brazing,^[13,14] and fusion welding,^[4,15] were used to join titanium alloy and stainless steel. Since fusion welding has higher flexibility in joint configurations, higher welding productivity, and easier preparation for welding,^[16] it is widely used in industrial production. The major challenge in fusion

welding of titanium alloy and stainless steel is the formation of hard and brittle IMCs in the weld, such as TiFe, $TiFe_2$, and $TiCr_2$,^[3,17] which would significantly increase the cracking susceptibility of the joint.^[18] Electron beam welding and laser welding are of high interest for joining titanium alloy and stainless steel due to their high energy density and precision of weld formation.^[19] Chen *et al.*^[20] investigated the direct laser butt welding of Ti-6Al-4V titanium alloy and 201 stainless steel, yielding durable joints only when the laser beam deflected to stainless steel. Wang *et al.*^[3,21] directly joined Ti6Al2Mo2V2Zr and TA15 titanium alloy to 304 stainless steel using electron beam welding. The resultant joints ruptured immediately, demonstrating the poor weldability between titanium alloy and stainless steel. From their reports, direct fusion welding of titanium alloy and stainless steel without interlayer materials is nearly impossible, even with high-energy beam welding technologies.

The interlayer for fusion welding of titanium alloy and stainless steel can be classified into three categories. Category I includes materials that do not react with both Ti and Fe, such as Mg. Gao *et al.*^[22] joined Ti-6Al-4V alloy and AISI 304L stainless steel using laser welding with an AZ31B Mg filler wire; the highest tensile strength of the resulting joints reached 221 MPa. Category II includes elements that form continuous solid solutions with Ti, such as V, Nb, Zr, and Ta.

XIAOHU HAO, PENG LI, YUEQING XIA, HONGGANG DONG, and PENGXIAO WANG are with the School of Materials Science and Engineering, Dalian University of Technology, Dalian 116024, P.R. China. Contact e-mail: donghg@dlut.edu.cn DEJUN YAN is with the Guangdong Provincial Key Laboratory of Advanced Welding Technology for Ships, CSSC Huangpu Wenchong Shipbuilding Company Limited, Guangzhou 510715, P.R. China

Manuscript submitted July 27, 2018.

Article published online November 29, 2018

However, Zr and Ta were seldom used to join titanium alloy and stainless steel due to the formation of various Zr-Fe IMCs and the high melting point of Ta (3293 K). Zhang *et al.*^[4] obtained a pulsed laser-welded joint between TC4 titanium alloy and 301L stainless steel with a tensile strength of 370 MPa using a 1-mm-thick pure Nb sheet as interlayer. Tomashchuk *et al.*^[23] reported that the tensile strength of a Ti6Al4V/AISI 316L laser-welded joint with a V sheet as an interlayer reached 367 MPa with a two-pass configuration.^[24] However, V is so sensitive to other elements (*e.g.*, Cr, Fe, H, O, and N) that the welding process with V as an interlayer demands more accurate welding control and stricter shielding.^[25,26] Category III consists of elements that form less brittle IMCs with Ti, where a typical example is Cu. On the one hand, Cu does not form brittle IMCs with Fe, Cr, or Ni,^[27] and Ti-Cu IMCs are less brittle than Ti-Fe IMCs. On the other hand, the excellent ductility of copper provides a compensating effect for the mismatched linear expansion coefficients of the base materials.^[28] It has been reported that the tensile strength of a laser-welded joint between Ti-15-3 alloy and 304 stainless steel reached 359 MPa when Cu was used as an interlayer.^[29]

The current study aims to explore the feasibility of using gas tungsten arc welding (GTAW) in joining TC4 titanium alloy and 304 stainless steel with a Cu-based filler wire. The evolution of the microstructure in the titanium substrate/weld transition zone and mechanical properties of the resultant butt joint were investigated with different welding parameters.

II. EXPERIMENTAL PROCEDURE

GTAW was used to join TC4 titanium alloy and 304 stainless steel with a Cu-based filler wire CuSi3 (1.2 mm outer diameter), and the effect of the filler wire on the microstructure and mechanical properties of the joint was investigated. The welding configuration and groove geometry are illustrated in Figures 1(a) and (b) through (h), respectively. The nominal composition of the base materials and filler wire are listed in Table I. The substrates were polished with SiC sandpapers and cleaned with alcohol before welding. Pure argon gas (99.99 pct) with a flow rate of 10 L/min was used to protect the liquid weld pool from air, and the top and back surfaces of the weld at elevated temperature were shielded with pure argon gas at flow rates of 15 and 8 L/min, respectively. The welding process was automatically performed using a YC500WX4N GTAW machine with a customized operating platform. The filler wire was uniformly fed into the weld pool with an electronic wire feeder. The arc position and detailed welding parameters are shown in Figure 1(b) through (h) and Table II, respectively. After conducting preliminary experiments, the arc was set at the center line of the butt gap to obtain stable joints with satisfactory appearance, as shown in Figure 1(h). With different grooves, the arc was moved to the edge of stainless steel to decrease the dissolution of titanium alloy.

The cross-sectional morphology in a TC4/304 SS joint without etching was observed using a confocal laser scanning microscope (OLS4000, OLYMPUS). The microstructure was examined using electron probe microanalysis (EPMA, JXA-8350F Plus, JEOL) with an electron beam size of 100 nm in the backscatter mode. Quantitative composition analysis was conducted to investigate the phase constitution. Elemental line scanning and mapping were also conducted with EPMA. The tensile properties of the TC4/304 SS butt joint were evaluated with a universal test machine (DNS-100) at a test rate of 1 mm/min. The dimensions and a typical photograph of a tensile test specimen are shown in Figure 2. The fractured surface was analyzed using a scanning electron microscope (SEM, Zeiss SUPRA55) equipped with an energy dispersive spectrometer (EDS). The Vickers microhardness in the Ti/weld transition zone was measured using an HV-1000B microhardness tester with 50 g load and 15 seconds dwell time. In order to determine the microhardness distribution in the Ti/weld transition zone, a microhardness test was conducted along two parallel lines separated by a distance of 50 μm across the Ti/weld transition zone. The distance between every two points was maintained at 50 μm , and the second line was shifted 25 μm to the right. The microhardness of the two lines merged into a single line when drawing the distribution curves, and the distance between every two points on the curve changed to 25 μm . In this way, the distance between every two tested points was larger than three times the diagonal length of the indentation; hence, the interaction between every two points can be ignored.

III. RESULTS

A. Macrostructure

The cross sections of the macrostructure in TC4/304 SS joints welded with different parameters are shown in Figure 3. A “C”-shaped Ti/weld transition zone (TZ) formed between the TC4 alloy substrate and the weld, and the width of transition zone generally increased as the welding current increased. Because the arc pointed to the edge of the 304 stainless steel, increasing the welding current led to a larger volume of melted stainless steel. Therefore, a certain amount of Fe inevitably entered the Ti/weld transition zone, resulting in the formation of Ti-Fe IMCs. In order to obtain a reliable TC4/304 SS joint, low welding heat input was required to suppress the formation of brittle IMCs. However, with low welding current or high traveling speed, serious undercut defects formed in samples B1 and B5. Figures 3(g) through (l) show the photos of the joints with different grooves. One can see that the rear appearance of the joints is much better with a symmetric V groove compared to the unilateral V groove on TC4 titanium alloy. Considering the continuity of the welding process and the tensile strength of the resulting joints, the symmetric V groove with a one-sided 30 deg angle and 1.0 mm root gap width (S30-1.0-T30) was

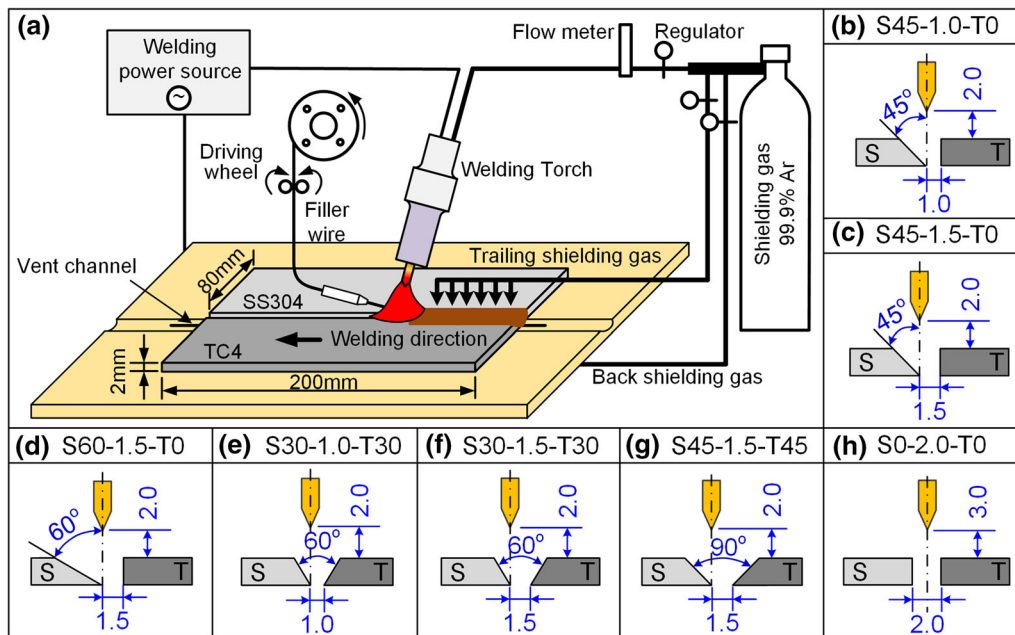


Fig. 1—Schematic diagram of (a) GTAW of TC4 titanium alloy and 304 stainless steel, and (b to h) their groove geometries.

Table I. Nominal Compositions of Base Materials and Filler Wire

Materials		Elements (Wt Pct)									
304 SS	C	Cr	Ni	Mn	Si	P	Cu	Mo	Ti	S	Fe
	≤ 0.08	18.07	8.112	1.15	0.418	0.023	0.021	0.018	0.003	0.003	bal.
Materials		Elements (Wt Pct)									
TC4	Al	V	Fe	Si	Ti						
	5.865	3.567	0.136	0.012							
Materials		Elements (Wt Pct)									
ERCuSi3	Si	Mn	Sn	Zn	Cu						
	2.8–4.0	≤ 1.5	≤ 1.0	≤ 1.0	bal.						

Table II. Parameters for GTAW of TC4 Titanium Alloy to 304 Stainless Steel

Sample No.	Groove type	Welding Current (A)	Traveling Speed (mm/s)	Wire feed Rate (mm/s)
B1	S0-2.0-T0	40	2	16
B2	(no groove)	50	2	16
B3		60	2	16
B4		80	2	18
B5		60	3	24
B6		80	3	24
B7		100	3	24
B8		120	3	24
P1	S30-1.0-T30	60	2	16
P2		60	3	24
P3		80	2	16
P4		80	3	24
P5		100	2	16
P6		100	3	24
P7		120	3	24
P8		120	4	30

confirmed as the preferred groove. A simultaneous increase in the welding current and traveling speed improved the weld appearance. However, more welding defects, such as cracks and voids, also formed in the resulting joint, as shown in Figures 3(m) through (o).

B. Microstructure

The distributions of elements in the inner and central areas of the top Ti/weld transition zone in sample B2 are shown in Figures 4(a) and (b), respectively. The Fe, Cr, and Ni contents were very low, indicating that the amount of melted 304 stainless steel substrate was very small, and almost no brittle Ti-Fe and Ti-Cr IMCs formed in the Ti/weld transition zone when the welding current was 50 A and the traveling speed was 2 mm/s. The dominant elements in the inner Ti/weld transition zone are Ti and Cu, which have nearly the same distribution, suggesting that various Ti-Cu IMCs formed during welding. Apart from Ti and Cu,

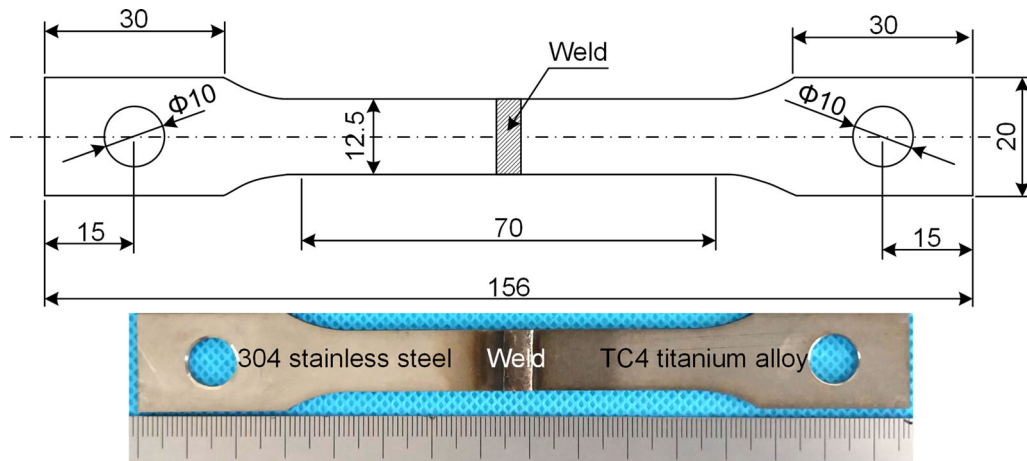


Fig. 2—Dimensions of tensile specimens. (Unit: mm).

segregation of Si was also found in the central Ti/weld transition zone, and more Ti was detected where Si was segregated. Moreover, segregation of an island-shaped Al block was observed. The distribution of V is similar to that of Ti due to the large mutual solubility between Ti and V.

The microstructures of the Ti/weld transition zone in the TC4/304 SS joint when the welding current was 50 A and the traveling speed was 2 mm/s (sample B2) are shown in Figure 5. A “C”-shaped transition zone formed near the TC4 alloy substrate. The top part of the TC4 titanium alloy substrate melted slightly, which then reacted with the liquid copper filler metal and formed a Ti/weld transition zone (see Figure 5(a)). Figures 5(b) through (c) show the microstructure of the middle and bottom areas of Ti/weld transition zones. There is no significant difference between the top, middle, and bottom regions, except that the distribution of black phases transformed from continuous in the top/middle region to discrete at the bottom. Figures 5(d) through (f) show the detailed microstructure of the top Ti/weld transition zone. The chemical composition of the featured positions is listed in Table III. Short rod-shaped black phases formed in the inner portion of the Ti/weld transition zone near the TC4 titanium alloy substrate, and the major elements in these phases were Ti and Cu with an atomic ratio of approximately 2:1. Therefore, these phases were deduced to be Ti_2Cu based on a Ti-Cu binary phase diagram.^[30] Bulk dark gray phases (labeled 3 and 5) formed near Ti_2Cu , and more Al was detected. These dark gray phases were identified as Ti_2Cu with a small amount of $AlCu_2Ti$ based on Al-Cu-Ti ternary phase diagram.^[31] The white phase (labeled 4) contained 12.84 at. pct Al at the boundary of dark gray phases, which was identified as a mixture of $AlCu_2Ti$ and $TiCu$ IMCs. A thin gray layer (labeled 6) formed near the TC4 titanium alloy substrate, which was deduced to be β -Ti based on the high contents of Al (10.04 at. pct) and Cu (11.36 at. pct). Outside the Ti_2Cu IMCs, needle-like Ti_2Cu and $AlCu_2Ti$ mixed IMCs (labeled 7) formed and grew vertically

toward the weld zone. The white phases (labeled 8) between the needle-like IMCs were considered to be $AlCu_2Ti$, which is consistent with the segregation of an island-shaped Al block in Figure 4. The microstructure is obviously finer in the central region than in the inner Ti/weld transition zone. Fine granulous $AlCu_2Ti$ (labeled 12) was distributed in the gray $TiCu$ matrix (labeled 11). Bulk light gray phases (labeled 10) and hexagonal black phases (labeled 13) formed in the central region of the Ti/weld transition zone. EPMA quantitative analysis reveals that the light gray phases are $AlCu_2Ti$ and the hexagonal black phases are Ti_5Si_3 . The Ti_5Si_3 phase remained segregated between the central region and outside the Ti/weld transition zone. The bulk gray phases outside the Ti/weld transition zone (labeled 14) were identified as $AlCu_2Ti$ with a small amount of $TiCu_4$. As shown in Figure 5(f), different phases formed at the boundary of $AlCu_2Ti$. Eutectic Ti_2Cu_3 and $TiCu_4$ (labeled 16) formed at the grain boundary of $AlCu_2Ti$ outside the Ti/weld transition zone, while $TiCu$ IMCs formed near the center of the Ti/weld transition zone.

EPMA line scanning analysis was conducted across the Ti/weld transition zone, and the elemental distribution is shown in Figure 5(g). The contents of Fe, Cr, and Ni in the Ti/weld transition zone are very low. The contents of both Ti and Al decreased, while the content of Cu increased as the distance from the TC4 titanium alloy substrate increased. Large fluctuations are present in the Ti, Al, Cu, and Si distribution curves, and the peak of the Ti curve corresponds with the troughs in the Cu and Si curves, indicating that discontinuous Ti-Cu and Ti-Si IMCs formed in the Ti/weld transition zone. The microstructure of the weld zone shows a typical equiaxed feature, as shown in Fig. 5(h). Due to the low welding heat input, a small amount of base materials was melted, and thus, an equiaxed ϵ -Cu solution formed in weld zone.

Figure 5(i) shows the microstructure of the weld/steel interface in the TC4/304 SS joint when the welding current was 50 A and the traveling speed was 2 mm/s. A

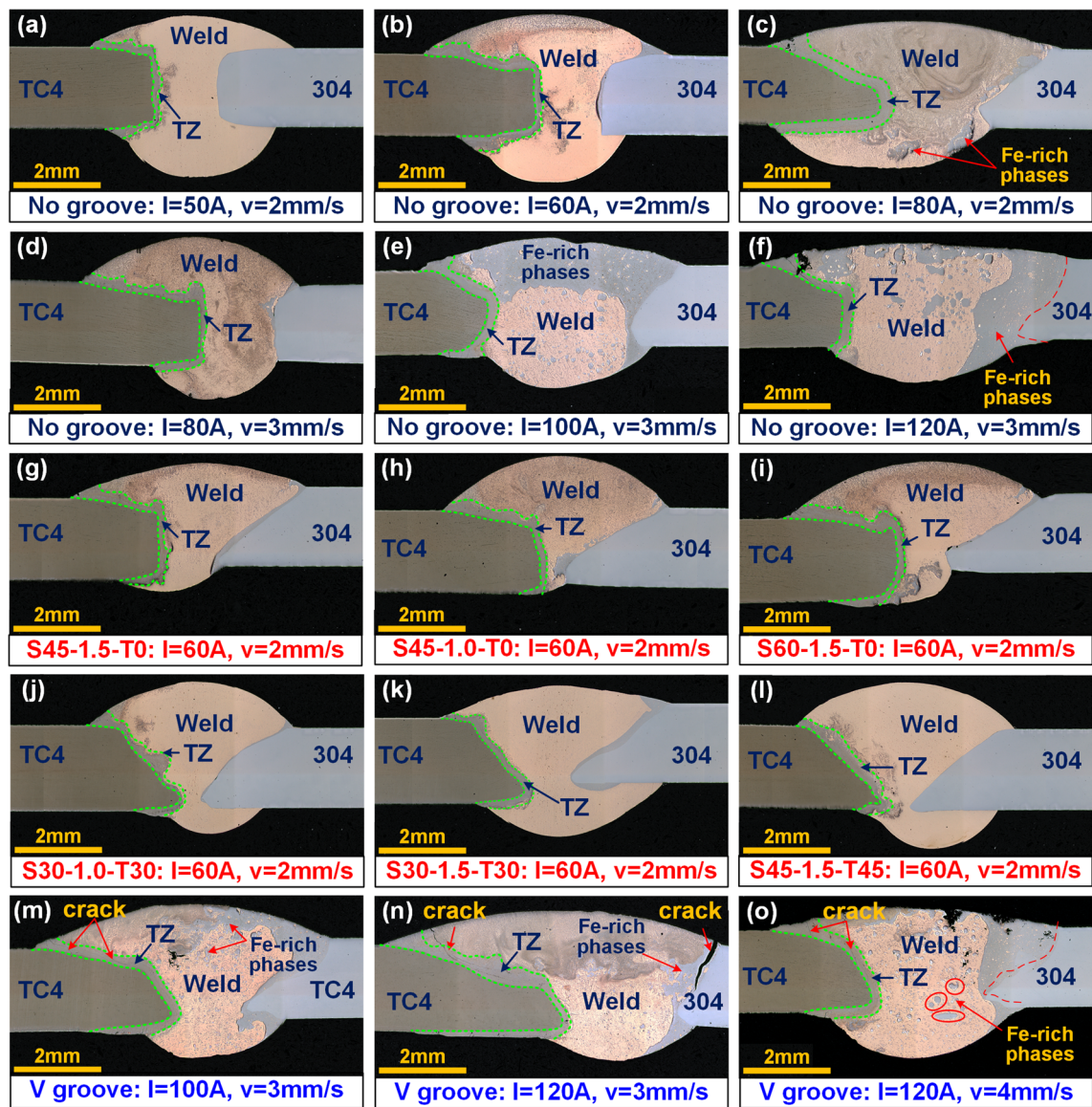


Fig. 3—Macrostructure of cross section in TC4/304 SS joint. (a) No groove, $I = 50$ A, $v = 2$ mm/s; (b) No groove, $I = 60$ A, $v = 2$ mm/s; (c) No groove, $I = 80$ A, $v = 2$ mm/s; (d) No groove, $I = 80$ A, $v = 3$ mm/s; (e) No groove, $I = 100$ A, $v = 3$ mm/s; (f) No groove, $I = 120$ A, $v = 3$ mm/s; (g) S45-1.5-T0 groove, $I = 60$ A, $v = 2$ mm/s; (h) S45-1.0-T0 groove, $I = 60$ A, $v = 2$ mm/s; (i) S60-1.5-T0 groove, $I = 60$ A, $v = 2$ mm/s; (j) S30-1.0-T30 groove, $I = 60$ A, $v = 2$ mm/s; (k) S30-1.5-T30 groove, $I = 60$ A, $v = 2$ mm/s; (l) S45-1.5-T45 groove, $I = 60$ A, $v = 2$ mm/s; (m) S30-1.0-T30 groove, $I = 100$ A, $v = 3$ mm/s; (n) S30-1.0-T30 groove, $I = 120$ A, $v = 3$ mm/s; (o) S30-1.0-T30 groove, $I = 120$ A, $v = 4$ mm/s.

thin dark layer of approximately $4 \mu\text{m}$ thickness formed between the weld zone and the 304 stainless steel substrate. The atomic fraction in the dark layers (marked with a cross) shows that 21 at. pct Si and 1.3 at. pct Ti are present in this layer, in addition to the major elements in 304 stainless steel. The EPMA line scanning results reveal that Si and Ti segregated in the weld/steel interface. A small amount of Ti was brought from the melted TC4 titanium alloy to the weld/steel interface due to fluid flow in the weld pool, which subsequently diffused into the 304 stainless steel substrate due to the relatively large chemical affinity between Fe and Ti. Si could dissolve into γ -Fe and form an interstitial solid solution due to the small

atomic radius of Si. Therefore, a diffusion weld/steel interface formed when the welding current was 50 A.

Figure 6 shows the microstructure of the TC4/304 SS joint when the welding current was 80 A and the traveling speed was 2 mm/s (sample B4). Micro cracks formed in the top of the Ti/weld transition zone due to the large mismatch between the thermal expansion coefficients. A significant content of bulk gray phases (labeled 1 and 2) formed in the inner region of the Ti/weld transition zone, and these phases were identified as ternary Ti-Cu-Fe IMCs with dissolved Al according to EPMA quantitative analysis. A thin β -Ti layer (labeled 3) was also observed in the joint welded with 50 A, which formed between the Ti-Cu-Fe IMCs and the TC4

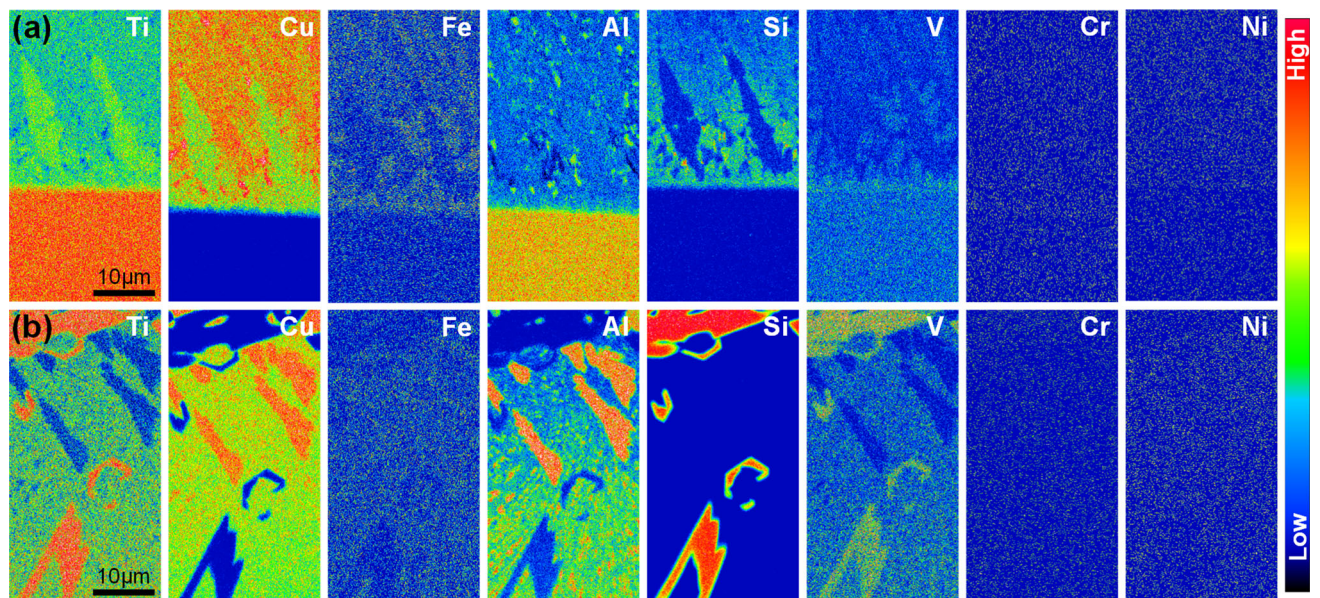


Fig. 4—Elemental distributions in the inner (a) and central (b) regions in top Ti/weld transition zone with welding current of 50 A and traveling speed of 2 mm/s.

titanium alloy substrate. Dark gray Ti_2Cu phases (labeled 4) and white $AlCu_2Ti$ phases (labeled 5) formed at the grain boundary of the Ti-Cu-Fe IMCs. The microstructure in the central region of the Ti/weld transition zone remarkably coarsened and the TiCu IMC disappeared in favor of $AlCu_2Ti$ (labeled 7, 9, and 10) and Ti-Cu-Fe IMCs (labeled 6). Similar to sample B2, Ti_5Si_3 dispersed in the central region of the Ti/weld transition zone with the decreasing size. Many dark gray phases precipitated at location 12 with high contents of Fe, Ti, Si, and Cr outside the Ti/weld transition zone, and they were regarded as complex quaternary Fe-Ti-Si-Cr IMCs. Among these Fe-Ti-Si-Cr IMCs, light gray $AlCu_2Ti$ phases (labeled as 11) and flower-like Ti-Cu-Fe IMCs (labeled 13) were also found at the grain boundary of the Fe-Ti-Si-Cr IMCs outside the Ti/weld transition zone.

The weld zone was composed of an ϵ -Cu solid solution matrix and dispersed black Fe-Ti-Si-Cr IMCs (labeled 15, 16 and 17). The titanium alloy and stainless steel were melted, and large amounts of Fe, Cr, and Ti dissolved into the weld and reacted with Si as the welding current increased, resulting in complex Fe-Ti-Si-Cr IMCs in the weld zone. A mushy zone developed in the weld/steel interface at a welding current of 80 A. As shown in Figure 6(h), the mushy zone consisted of a dark gray Fe-Ti-Si-Cr-Ni phase (labeled 18), light gray Fe-Cr-Ni solution (labeled 19), and white ϵ -Cu solid solution. Ti and Si atoms could easily diffuse into this mushy zone and react with Fe, Cr, and Ni, forming the complex Fe-Ti-Si-Cr-Ni phases.

With a simultaneous increase of welding current and traveling speed, the microstructure of the Ti/weld transition zone in TC4/304 SS joint with the optimized V groove is similar to that in sample B4, as shown in Figure 7. The inner Ti/weld transition zone consisted of large bulk Ti-Cu-Fe IMCs, and $AlCu_2Ti$ with Ti_2Cu

formed at the grain boundary of the Ti-Cu-Fe IMCs. Ternary Ti-Cu-Fe IMCs were distributed in the $AlCu_2Ti$ matrix within the central region of the Ti/weld transition zone. Dispersed bulk dark Fe-Ti-Si-Cr IMCs phases (labeled 7 and 13) formed outside of the Ti/weld transition zone because more Fe and Cr dissolved into the weld pool and migrated toward the TC4 alloy side when the welding current was high. An appropriate V groove can only improve the rear appearance of TC4/304 SS butt joints, yet it has little effect on the microstructure of the Ti/weld transition zone.

C. Tensile Properties and Fracture Analysis

The tensile strengths of the TC4/304 SS joint with different welding parameters are shown in Figure 8. The joint with a welding current of 40 A and traveling speed of 2 mm/s broke during the machining process, and a similar phenomenon occurred in the sample with a welding current of 60 A and traveling speed of 3 mm/s. With lower welding current and higher traveling speed, serious undercut defects appeared, and kiss bonding occurred in the TC4/304 SS joint. The tensile strength of the TC4/304 SS joint reached the maximum value of 290 MPa at a welding current of 50 A and traveling speed of 2 mm/s, followed by a slight decrease to around 250 MPa as the welding current increased to 60 and 80 A. Similar variation in tensile strength with the welding current occurred when traveling speed was 3 mm/s. The maximum tensile strength of the TC4/304 SS joint was 281 MPa when the traveling speed was 3 mm/s. This shows that the tensile strength of the joint decreases with increased welding current. Microstructure analysis showed that increased welding current caused brittle Ti-Cu-Fe IMCs to form in the Ti/weld transition zone, thus deteriorating the tensile strength. The tensile strength data became discretized accordingly due to

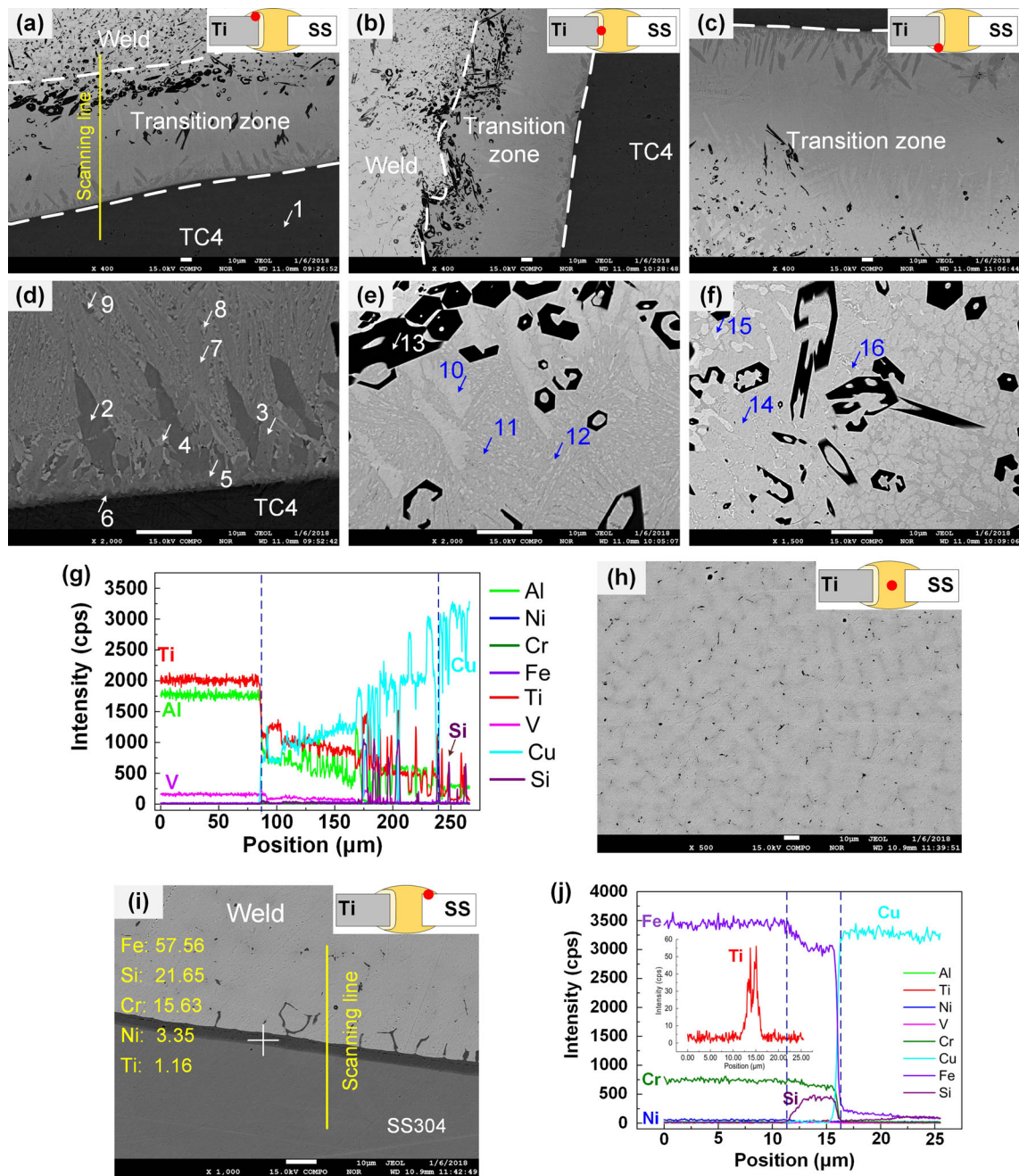


Fig. 5—Microstructures of TC4/304 SS joint (sample B2) welded with welding current of 50 A and traveling speed of 2 mm/s. (a through f) Ti/weld transition zone, (g) elements line scanning analysis in top Ti/weld transition zone, (h) weld zone, (i) weld/steel interface, (j) elements line scanning analysis in weld/steel interface.

more discontinuous micro cracks in the brittle Ti/weld transition zone as the welding current increased. This is also the main reason for the reduced tensile strength when the welding current increased from 80 to 100 A.

Figure 8(c) shows the effect of the groove geometry on the tensile strength of the TC4/304 SS joint. All joints were formed with a welding current of 60 A, except for sample S45-1.5-T0(II), which was welded with a welding current of 50 A, as marked in Figure 8(c). One can see that the tensile strength of the joints is higher with a symmetric V groove compared to the unilateral V

groove. On one hand, a symmetric V groove contributes to better rear appearance, which increases the tensile strength of the resulting joint. On the other hand, the dissolution of titanium alloy with a symmetric V groove is less than with a unilateral V groove; thus, the amount of brittle Ti-rich IMCs decreased, and the tensile strength of the resulting joints increased. Moreover, the decreased groove angle and gap width improved the tensile strength. This can be attributed to incomplete filling of groove defects while using a large groove angle and gap width.

Table III. EPMA Quantitative Analysis Results in TC4/304 SS Joint (Sample B2)

Position	Elements (At. Pct)								Possible Phases
	Al	Ti	Si	Cr	Ni	Cu	V	Fe	
1	10.23	85.66	0.04	0.10	—	0.06	3.79	0.12	$\alpha + \beta$ Ti
2	5.81	60.93	0.55	0.06	—	29.87	2.63	0.15	Ti ₂ Cu
3	6.43	53.18	2.57	0.13	—	32.45	4.53	0.70	Ti ₂ Cu + AlCu ₂ Ti
4	12.84	33.48	0.81	—	—	51.84	0.92	0.11	AlCu ₂ Ti + TiCu
5	6.77	55.56	2.57	0.14	—	29.22	5.00	0.74	Ti ₂ Cu + AlCu ₂ Ti
6	10.04	72.06	0.65	0.13	—	11.36	5.46	0.30	β -Ti
7	6.05	52.00	1.61	0.08	—	35.95	3.74	0.57	Ti ₂ Cu + AlCu ₂ Ti
8	12.30	36.59	0.40	0.04	—	49.28	1.21	0.18	AlCu ₂ Ti
9	6.53	57.72	0.59	0.03	—	32.81	2.16	0.16	Ti ₂ Cu
10	11.03	28.10	0.06	0.04	—	60.15	0.38	0.24	AlCu ₂ Ti
11	3.87	47.65	0.44	0.09	—	45.48	2.01	0.45	TiCu
12	9.66	34.25	0.26	0.03	—	54.53	0.94	0.33	AlCu ₂ Ti
13	0.11	57.91	35.55	0.14	—	0.89	5.30	0.09	Ti ₅ Si ₃
14	5.49	26.71	0.14	—	—	67.11	0.34	0.22	AlCu ₂ Ti + TiCu ₄
15	1.88	11.24	0.02	—	—	86.40	0.28	0.17	ϵ -Cu
16	0.49	35.99	0.18	0.16	—	60.47	1.65	1.07	Ti ₂ Cu ₃ + TiCu ₄

With the preferred symmetric V groove (S30-1.0-T30), different welding currents and speeds were optimized to further improve the tensile strength of the TC4/304 SS joint. As shown in Figure 8(d), the tensile strength of all other joints increased with the increasing traveling speed, except for the joints welded at 80 A. A maximum tensile strength of 328 MPa was obtained with a welding current of 120 A and traveling speed of 4 mm/s. The large fluctuations in the tensile strength data can be attributed to randomly formed cracks and heterogeneity of the microstructure in the Ti/weld transition zone (Table IV).

The fracture surfaces on the titanium alloy side of the joints were examined with an SEM after conducting the tensile test. The presence of cleavage features suggests the joints are brittle. As shown in Figure 9, cracks appeared in the fracture surfaces on the TC4 titanium alloy side, and propagated perpendicularly to the welding direction. The generation of cracks is attributed to the large difference in thermophysical properties, such as coefficients of linear expansion and thermal conductivity. The fracture surface from the joint with a tensile strength of 290 MPa is shown in Figure 9(a), and the morphology of the fracture surface is similar to the needle-like microstructure in the Ti/weld transition zone (in Figure 5). A river-like pattern, which is typical of the cleavage fracture mode, can be seen on the fracture surface on the titanium alloy side, and the EDS results (Table V) suggest that fracture occurred through Ti₂Cu and AlCu₂Ti IMCs. The fracture surface of the joint formed with higher welding current (sample B8, 120 A) is shown in Figure 9(b). Lamellar cleavage planes appeared on the fracture surface, and the EDS results show that rupture occurred through Ti₂Cu and AlCu₂Ti IMCs in the Ti/weld transition zone. Similar fracture features appeared with the V groove in Figure 9(c), suggesting that the V groove had little effect on the fracture mode. However, IMC grains and the grain boundary can be found on the fracture surface in

Fig. 9(d) when the welding current was 120 A and traveling speed was 4 mm/s, and the intergranular fracture mode dominated the rupture process. EDS results reveal that ternary Ti-Cu-Fe IMCs formed inside the grains and complex Fe-Ti-Si-Cr-Cu IMCs formed at the grain boundary. This agrees with the microstructure analysis discussed before. It was reported that Ti-Cu-Fe IMCs have low crack resistance,^[32] and ruptures would prefer to propagate through the Ti-Cu-Fe IMCs.

D. Microhardness

The effects of welding current and traveling speed on the microhardness distribution across the middle of the Ti/weld transition zone are illustrated in Figure 10. The microhardness in the TC4 titanium alloy remained stable from the base metal to the heat-affected zone (HAZ), demonstrating that no significant microstructure changes occurred in the HAZ on the TC4 titanium alloy side. As shown in Figure 10, the microhardness in the Ti/weld transition zone sharply increased above 500 HV, and the peak microhardness reached 619 HV (Figure 10(e)). The variation of microhardness was closely related to the microstructure of the Ti/weld transition zone. Actually, Ti₂Cu, TiCu, Ti₅Si₃, AlCu₂Ti, Ti-Cu-Fe phases, and other complex IMCs with high microhardness formed in the Ti/weld transition zone, resulting in the obvious increase in microhardness. The average microhardness of the Ti/weld transition zone increased as the welding current increased when the traveling speed was kept constant at 2 mm/s. This phenomenon is attributed to the inclusion of more Fe and Cr in the Ti/weld transition zone, followed by reaction with Ti, Cu, and Si as the welding current increased, resulting in the formation of Ti-Cu-Fe and Fe-Ti-Si-Cr IMCs with high microhardness. When welded with 80 A at 2 mm/s, the microhardness of the Cu weld is higher than in other joints, and the fluctuation is also larger. Dissolution of substrates

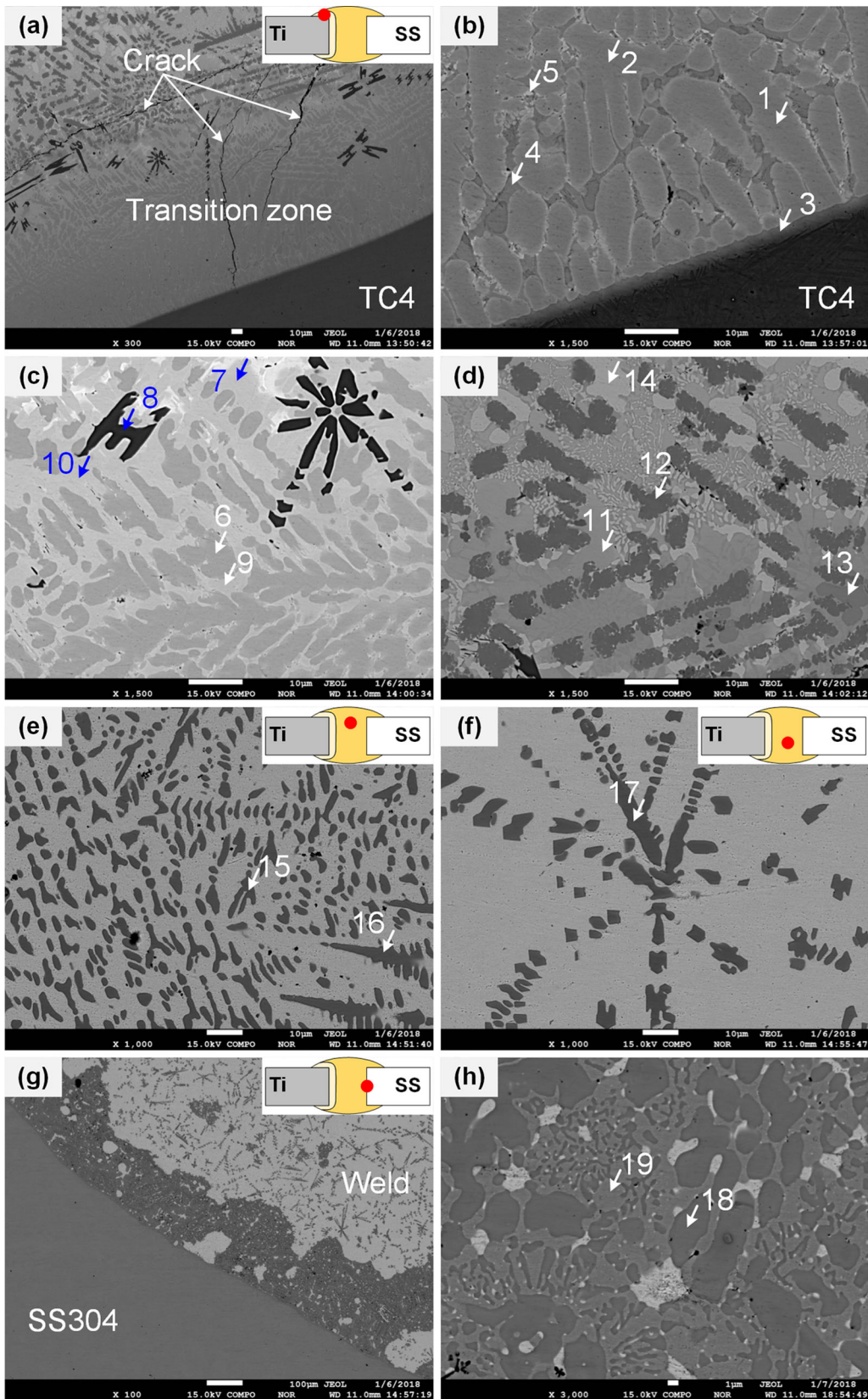


Fig. 6—Microstructures of Ti/weld transition zone (*a* through *d*), weld (*e*, *f*), and weld/steel interface (*g*, *h*) in TC4/304 SS joint with welding current 80 A and traveling speed 2 mm/s.

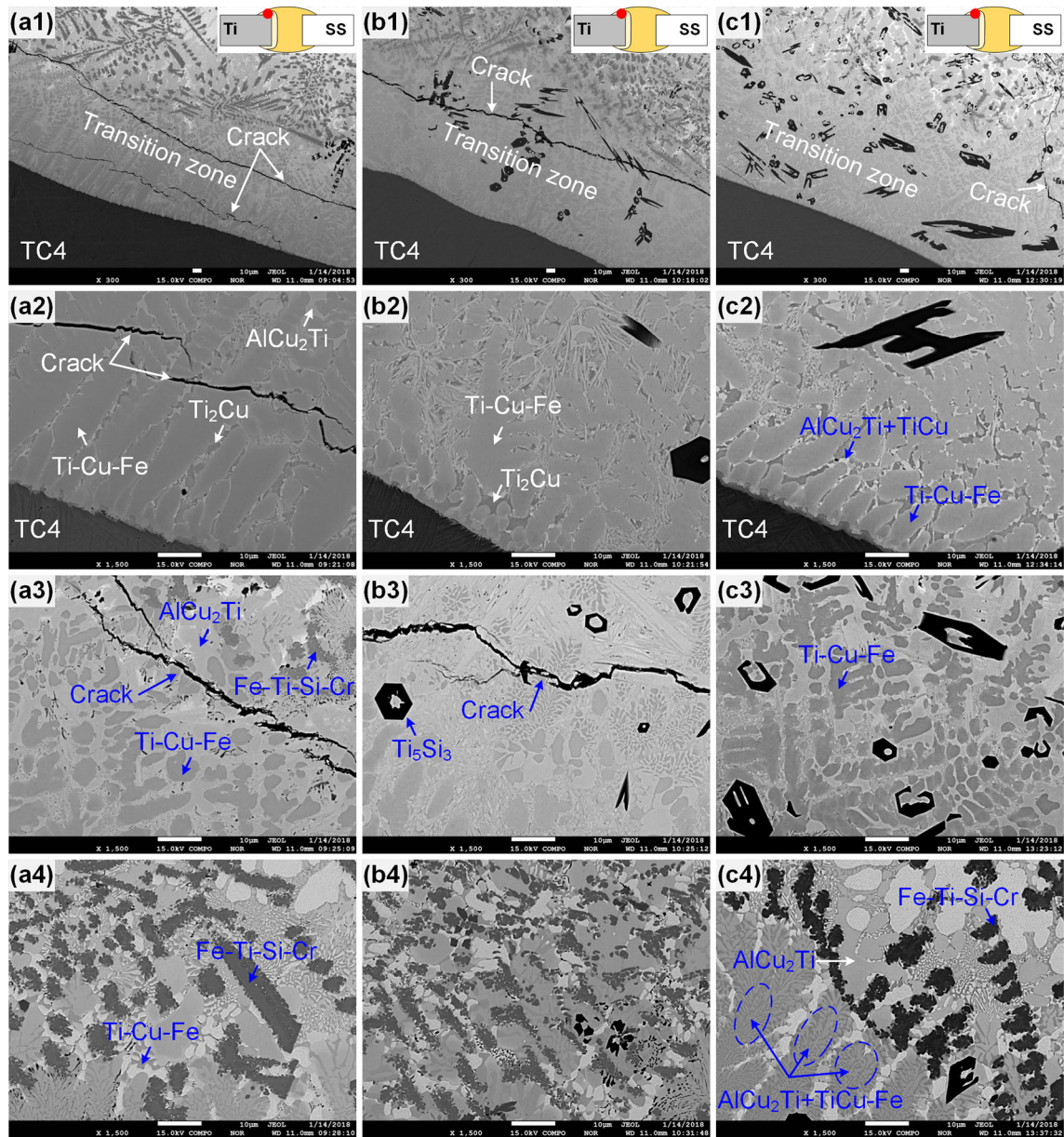


Fig. 7—Microstructures of Ti/weld transition zone in TC4/304 SS joint with symmetric V groove (S30-1.0-T30). (a1 through a4) Sample P6 welded at 100 A and 3 mm/s; (b1 through b4) sample P7 welded at 120 A and 3 mm/s; (c1 through c4) sample P8 welded at 120 A and 4 mm/s.

increased with high welding heat input and could explain this phenomenon, where more Ti, Fe, and Cr entered the weld pool, followed by the formation of complex Fe-Ti-Si-Cr IMCs and dispersion strengthening in the weld.

IV. DISCUSSION

A. Microstructural Evolution

Less than 0.1 at. pct Fe can dissolve into α -Ti at room temperature.^[33] Brittle TiFe (~ 600 HV) and TiFe₂ (~ 1000 HV) IMCs would easily form.^[17] In this study, Cu-based filler wire was used to prevent the formation of brittle TiFe and TiFe₂ IMCs in the TC4/304 SS joint.

In order to minimize fusion of the TC4 titanium alloy, the arc was pointed toward the edge of the 304 stainless steel. However, the TC4 titanium alloy substrate still slightly dissolved due to the arc heat and Ti-Cu eutectic reaction. When the welding current was 40 A and the traveling speed was 2 mm/s, or when the welding current was 60 A and the traveling speed was 3 mm/s, the TC4 titanium alloy substrate remained almost entirely solid, and weak bonding occurred between TC4 titanium alloy and 304 stainless steel. Figure 8 shows that the corresponding joint failed before the tensile test. Increasing the welding current to 50 A with 2 mm/s traveling speed produced a reliable joint with an average tensile strength of 290 MPa. TC4 titanium alloy dissolved slightly and then reacted with the liquid copper filler metal, resulting in a Ti/weld transition zone between the TC4 substrate

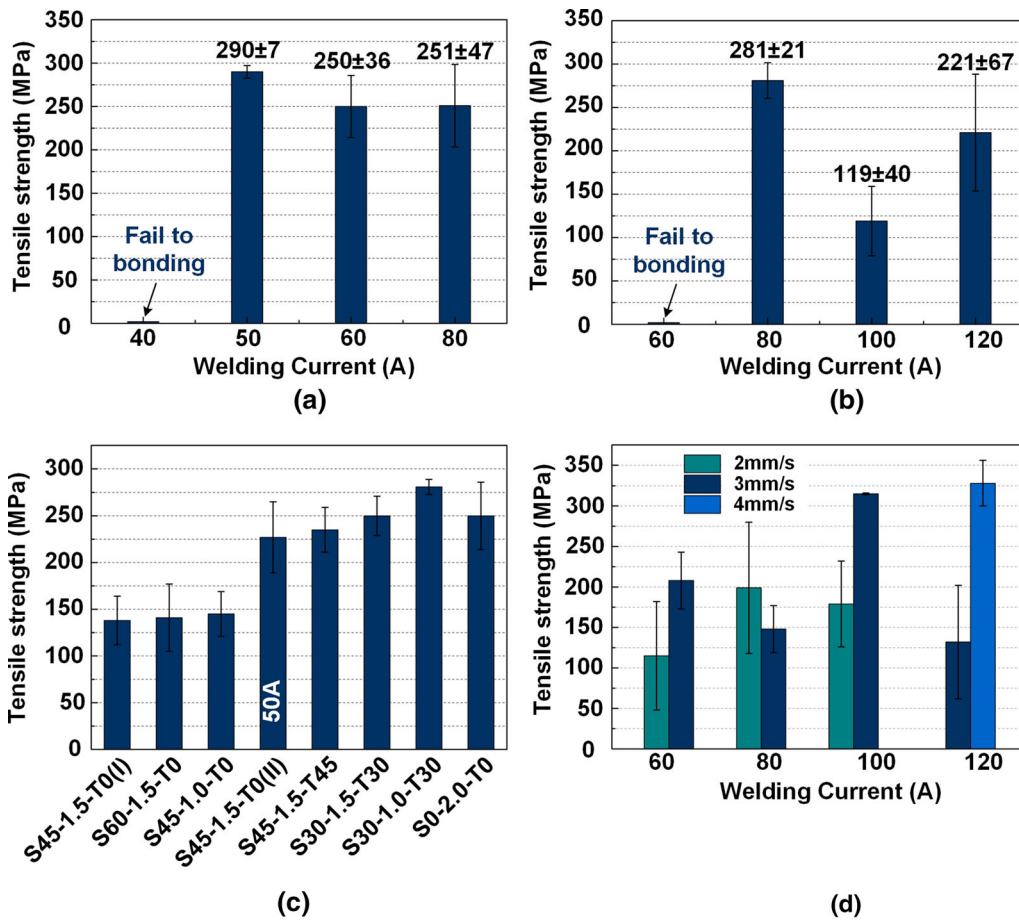


Fig. 8—Tensile strengths of TC4/304 SS joints welded with (a) traveling speed 2 mm/s, (b) traveling speed 3 mm/s, (c) different groove geometry, and (d) symmetrical V groove (S30-1.0-T30) with higher welding current.

Table IV. EPMA Quantitative Analysis Results in TC4/304 SS joint (Sample B4)

Position	Elements (At. Pct)									Possible Phases
	Al	Ti	Si	Cr	Ni	Cu	V	Fe		
1	7.21	55.33	2.04	1.55	0.84	21.27	4.13	7.64	Ti-Cu-Fe	
2	6.92	54.13	1.99	1.71	0.74	22.34	3.95	8.23	Ti-Cu-Fe	
3	9.78	73.32	0.70	0.64	0.06	8.89	4.45	2.15	β -Ti	
4	5.66	63.00	0.55	0.09	0.46	28.50	1.27	0.48	Ti ₂ Cu	
5	11.87	38.48	0.37	0.15	1.15	46.31	0.95	0.71	Ti ₂ Cu + AlCu ₂ Ti	
6	3.66	48.59	2.06	1.91	1.23	29.85	2.21	10.48	Ti-Cu-Fe	
7	11.15	27.73	0.09	0.25	0.78	58.27	0.33	1.40	AlCu ₂ Ti	
8	0.24	56.89	32.97	1.60	—	1.96	5.31	1.02	Ti ₅ Si ₃	
9	13.79	28.27	0.05	0.18	1.08	54.84	0.45	1.35	AlCu ₂ Ti	
10	11.56	27.92	—	0.22	0.83	57.55	0.35	1.56	AlCu ₂ Ti	
11	6.69	26.47	0.17	0.14	1.21	62.89	0.21	2.21	AlCu ₂ Ti	
12	0.12	30.36	16.51	8.44	2.83	2.88	1.69	37.16	Fe-Ti-Si-Cr	
13	2.47	46.44	1.63	0.95	2.74	30.15	0.62	15.00	Ti-Cu-Fe	
14	3.65	7.66	0.02	0.15	—	87.49	0.07	0.97	ϵ -Cu	
15	0.05	28.77	15.62	8.51	4.08	2.62	1.43	38.93	Fe-Ti-Si-Cr	
16	0.04	27.87	15.88	8.58	3.30	2.52	1.42	40.39	Fe-Ti-Si-Cr	
17	0.06	26.36	14.48	8.94	3.63	2.29	0.92	43.31	Fe-Ti-Si-Cr	
18	0.04	24.50	12.66	9.99	4.90	0.74	0.76	45.41	Fe-Ti-Si-Cr-Ni	
19	0.21	2.59	3.50	20.03	6.57	2.75	1.01	63.34	Fe-Cr-Ni	

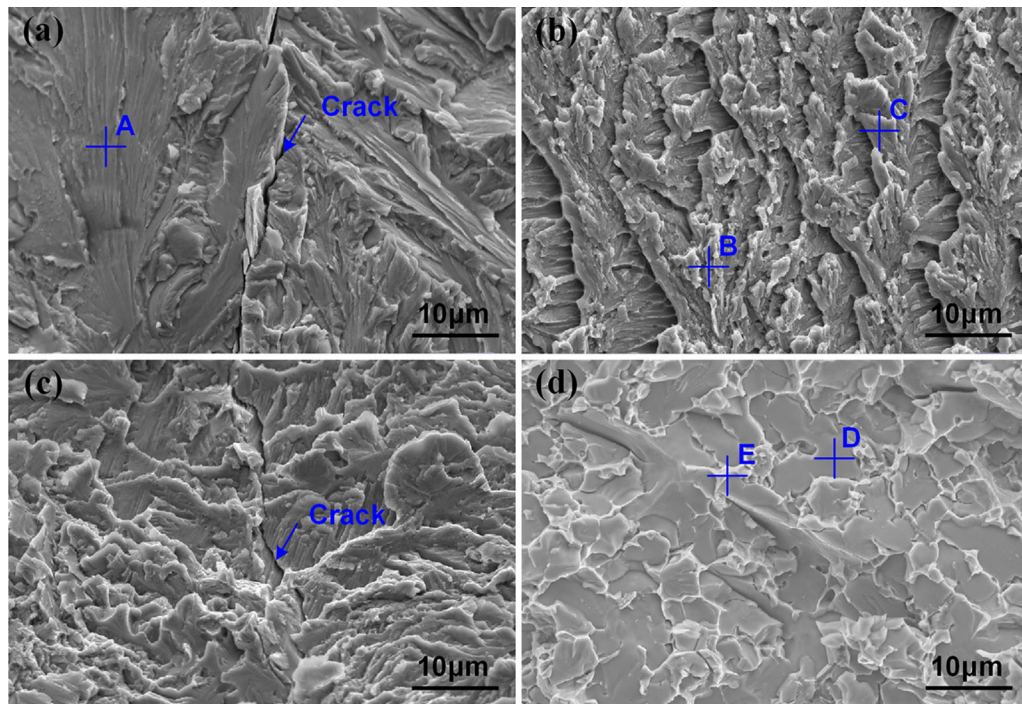


Fig. 9—Fracture surfaces on titanium alloy side of TC4/304 SS joint. (a) sample B2, welding current 50 A, traveling speed 2 mm/s, no groove; (b) sample B8, welding current 120 A, traveling speed 3 mm/s, no groove; (c) sample P6, welding current 100 A, traveling speed 3 mm/s, S30-1.0-T30 groove; (d) sample P8, welding current 120 A, traveling speed 4 mm/s, S30-1.0-T30 groove.

Table V. Chemical Compositions of Corresponding Locations in Fracture Surface of TC4/304 SS Joint

Position	Elements (At. Pct)								Possible Phases
	Al	Ti	Si	Cr	Ni	Cu	V	Fe	
A	4.77	38.20	1.12	—	—	53.80	2.21	0.12	Ti ₂ Cu + AlCu ₂ Ti
B	8.17	57.24	0.81	—	0.08	29.56	3.35	0.93	Ti ₂ Cu
C	6.66	51.25	0.50	—	0.47	39.46	1.58	0.11	Ti ₂ Cu + AlCu ₂ Ti
D	0.83	14.73	8.02	6.42	4.16	34.57	0.57	30.70	Ti-Cu-Fe
E	0.37	23.09	11.39	10.31	2.70	9.09	0.85	42.20	Fe-Ti-Si-Cr-Cu

and the weld. A thin layer of β -Ti formed adjacent to the solid TC4 substrate. A similar β -Ti layer was also found with higher welding current, and the thickness of the β -Ti layer increased as the welding current increased. The formation of β -Ti resulted from the diffusion of Cu into the TC4 titanium alloy substrate at elevated temperatures. Increasing the welding current could accelerate the diffusion of Cu, resulting in the formation of a thicker β -Ti layer.

Figure 11 shows the solidification sequence and formation of IMCs in the Ti/weld transition zone when the welding current was 50 A and the traveling speed was 2 mm/s. Nonequilibrium solidification occurred in the weld pool, and the nucleation and growth of all IMCs proceeded quickly. Ti₅Si₃ phases with a high melting temperature of 2403 K nucleated and grew outside the Ti/weld transition zone. From a thermodynamics perspective, the formation enthalpy (ΔH) of the Ti-Si system is lower than that of the Ti-Cu system when the

mass fraction of Ti is less than 80 pct.^[34] Therefore, Ti₅Si₃ phases formed first outside the Ti/weld transition zone. Ternary AlCu₂Ti phases nucleated and grew around the Ti₅Si₃ phase when the temperature in the Ti/weld transition zone decreased to 1373 K. Meanwhile, AlCu₂Ti nucleated within the Ti/weld transition zone due to the flow of the weld pool, resulting in the restricted growth of AlCu₂Ti, followed by the formation of granular AlCu₂Ti within the central region of the Ti/weld transition zone. A peritectic reaction of $L + \beta\text{-Ti} \rightarrow \text{Ti}_2\text{Cu}$ occurred at 1278 K with further cooling, and Ti₂Cu nucleated on the surface of AlCu₂Ti. Ti₂Cu grew quickly with a short rod-shaped morphology appearing toward the weld due to the large temperature gradient near β -Ti. When the temperature dropped to 1255 K, TiCu began forming around the granular AlCu₂Ti, and a small amount of Ti₃Cu₄ may also form *via* the peritectic reaction of $L + \text{TiCu} \rightarrow \text{Ti}_3\text{Cu}_4$ when the temperature was lower than 1198 K. Finally, the

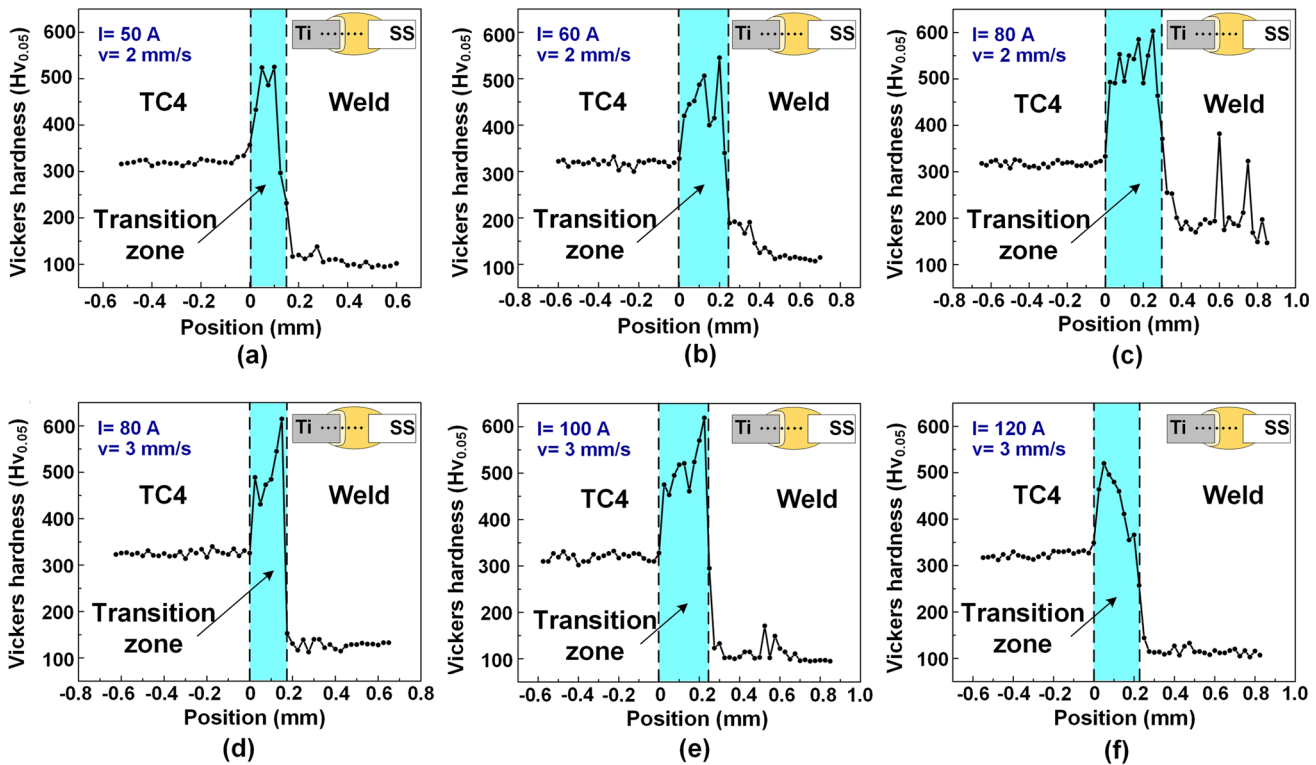


Fig. 10—Microhardness distributions in Ti/weld transition zone in TC4/304 SS joints. (a) No groove, $I = 50$ A, $v = 2$ mm/s; (b) No groove, $I = 60$ A, $v = 2$ mm/s; (c) No groove, $I = 80$ A, $v = 2$ mm/s; (d) No groove, $I = 80$ A, $v = 3$ mm/s; (e) No groove, $I = 100$ A, $v = 3$ mm/s; (f) No groove, $I = 120$ A, $v = 3$ mm/s.

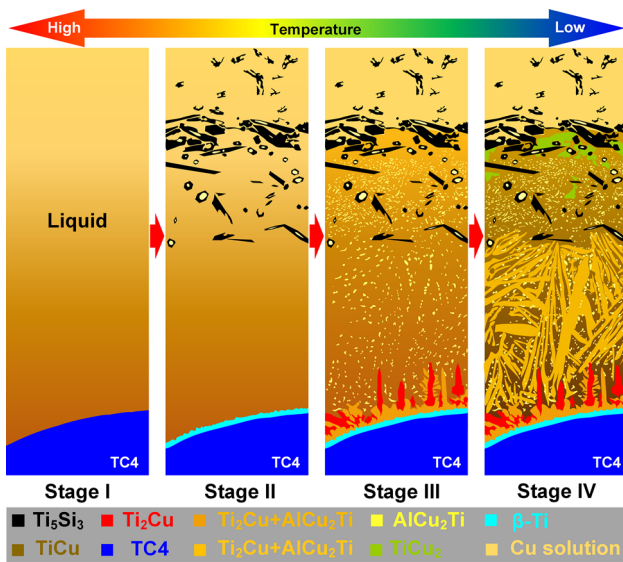


Fig. 11—Schematic diagram of solidification process in Ti/weld transition zone with lower welding current (sample B2, 50 A).

residual liquid transformed into metastable $TiCu_2$ and $TiCu_4$, and metastable $TiCu_2$ would decompose into Ti_2Cu_3 and $TiCu_4$ via the eutectoid reaction $TiCu_2 \rightarrow Ti_2Cu_3 + TiCu_4$.

The solidification process in the Ti/weld transition zone with a welding current of 80 A and traveling speed of 2 mm/s is shown in Figure 12. As discussed above, more Fe and Cr were detected in the Ti/weld transition zone. The aforementioned segregation of Ti_5Si_3 outside the Ti/weld transition zone disappeared, and bulk dark gray Fe-Ti-Si-Cr IMCs formed instead. Due to the increased welding current, the volume of melted stainless steel and the amounts of Fe and Cr in the weld zone both increased. Moreover, the increasing welding current would accelerate the flow of the weld pool, resulting in the disappearance of Ti_5Si_3 and growth of complex Fe-Ti-Si-Cr IMCs. Bulk Ti-Cu-Fe IMCs formed in the Ti/weld transition zone when a large welding current was used. Based on the Miedema model,^[35] the formation enthalpy of the Ti-Fe system is lower than that of the Ti-Cu system; thus, Ti-Fe IMCs would form prior to Ti-Cu IMCs. One can infer that $TiFe_x$ ($TiFe$ or $TiFe_2$) phases nucleated as precursor, followed by the diffusion of Cu into $TiFe_x$ IMCs. It has been reported that as much as 38 at. pct Cu could dissolve into cubic $TiFe$.^[36] The $TiFe_x$ precursor also caused the nucleation of Ti_2Cu . As a result, ternary Ti-Cu-Fe IMCs formed in the inner region of the Ti/weld transition zone adjacent to the TC4 substrate with diffusion of Cu and nucleation of Ti_2Cu around $TiFe_x$ particles. Subsequently, a small amount of residual liquid still existed between IMCs, finally transforming to $AlCu_2Ti$ upon further cooling.

Two different types of weld/steel interfaces formed as the welding current increased. A small amount of 304 stainless steel melted, and the end face of the 304 stainless steel remained solid when the welding current was 50 A. Liquid Cu filler metal with a certain amount of Ti wetted the 304 stainless steel, and the diffusions of

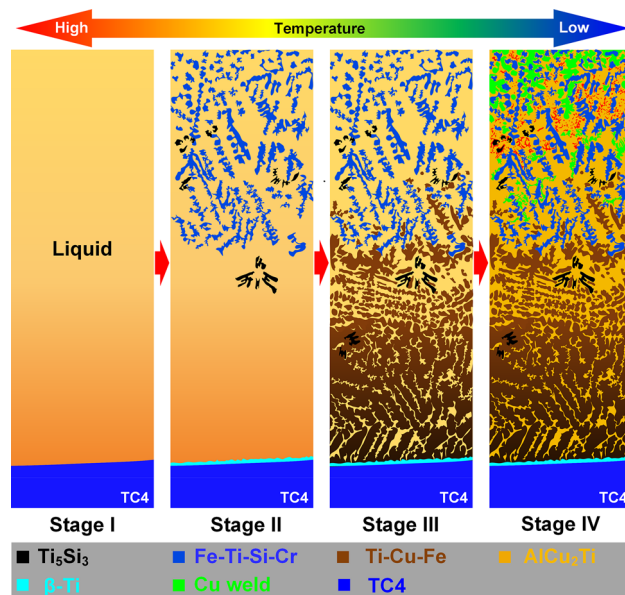


Fig. 12—Schematic diagram of solidification process in Ti/weld transition zone with higher welding current (sample B4, 80 A).

Si and Ti into the stainless steel substrate occurred in the weld/steel interface, resulting in a solid-state weld/steel interface. Increasing the welding current would obviously promote the fusion of stainless steel. The edge of 304 stainless steel completely melted, and a mushy zone formed in the weld/steel interface. Diffusions of Ti and Si in this mushy zone were easier than that in solid 304 stainless steel; hence, more Ti and Si diffused into mushy zone, resulting in the formation of complex Fe-Ti-Si-Cr-Ni phases.

B. Cracking of TC4/304 SS Joint

It was reported that a direct laser-welded joint of titanium alloy and stainless steel without an interlayer would rupture spontaneously,^[20] and the GTAW joint between TA15 titanium alloy and 18-8 stainless steel using an HS227 Cu-based filler wire also cracked in the weld metal.^[37] The results presented here show that cracks formed easily in the TC4/304 SS joint, especially when the welding current was high. This was the main reason for the low tensile strength of the TC4/304 SS joint welded with high welding current. Figure 13 shows longitudinal cracks in the Ti/weld transition zone and transverse cracks in the weld. The formation of cracks in the TC4/304 SS joint was attributed to the brittle Ti/weld transition zone and the large welding residual stress caused by the difference in thermophysical properties among TC4 titanium alloy, 304 stainless steel, and Cu. The thermophysical properties of the substrates and Cu filler metal are listed in Table VI.^[38] Longitudinal cracks

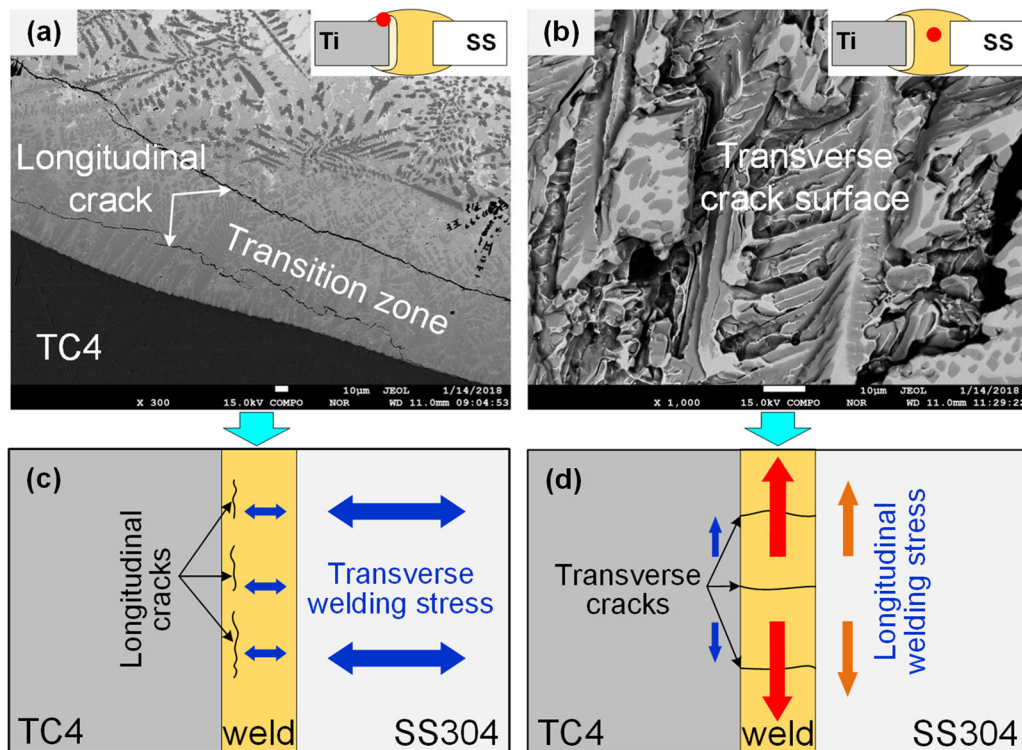


Fig. 13—Cracks in the cross section of TC4/304 SS joint. (a) Longitudinal cracks in Ti/weld transition zone, (b) transverse cracks in weld, formation mechanism of (c) longitudinal cracks and (d) transverse cracks.

Table VI. Thermophysical Properties of Base Materials and Copper-Based Filler Wire

Alloy	Specific Heat (J kg ⁻¹ K ⁻¹)	Thermal Conductivity (W m ⁻¹ K ⁻¹)	Linear Expansion Coefficient (10 ⁻⁶ K ⁻¹)
TC4 titanium alloy	526.3	6.7	8.6
304 stainless steel	500	16.2	17.3
Copper	380	36.0	18.0

propagating in the Ti/weld transition zone along the welding direction resulted from transverse welding stress induced by the large linear expansion coefficients of 304 stainless steel and the CuSi3 filler metal. Transverse cracks were caused by longitudinal shrinkage mismatch among TC4 titanium alloy, 304 stainless steel, and weld metal. The localized temperature of TC4 titanium alloy substrate near the weld was much lower than that of 304 stainless steel and the weld due to the lower thermal conductivity and larger specific heat of TC4 titanium alloy. The linear expansion coefficient of TC4 titanium alloy is much lower than that of the other two materials; therefore, the shrinkage of TC4 titanium alloy was the smallest, while that of the weld was the largest. Therefore, longitudinal shrinkage of the Cu weld and 304 stainless steel was restricted by TC4 titanium alloy. This is the root cause of the longitudinal welding stress. Transverse cracks formed in the weld when the longitudinal welding stress was greater than the tensile strength of the Cu weld.

V. CONCLUSIONS

- (1) TC4 titanium alloy was welded with 304 stainless steel using GTAW with a CuSi3 filler wire. Without a groove, the tensile strength of the TC4/304 SS joint reached 290 MPa when the welding current was 50 A and the traveling speed was 2 mm/s. With a symmetric V groove, the tensile strength of the joint reached 328 MPa when the welding current was 120 A and the traveling speed was 4 mm/s. Using an increased welding current resulted in the decreased tensile strength because more brittle IMCs and cracks formed in the joint. Simultaneously increasing the welding current and traveling speed improved the tensile strength of the joint. Cracks in the Ti/weld transition zone and Cu weld restricted further improvement of tensile strength.
- (2) The Ti/weld transition zone was composed of β -Ti, Ti₂Cu, AlCu₂Ti, TiCu, and Ti₅Si₃ IMCs when the welding current was 50 A. The weld consisted of an equiaxed ϵ -Cu solution. Si and Ti diffused into 304 stainless steel, resulting in a uniform weld/steel interface. Increasing the welding current resulted in formation of ternary Ti-Cu-Fe IMCs in the Ti/weld transition zone. The segregation of Ti₅Si₃ IMCs obviously decreased, and bulk complex Fe-Ti-Si-Cr IMCs formed in the Ti/weld transition zone. The preferred symmetric V groove could only improve

the appearance of the TC4/304 SS joint, and had little effect on the microstructure of the Ti/weld transition zone.

- (3) The microhardness in the Ti/weld transition zone was much higher than that in the TC4 substrate and Cu weld due to the formation of massive IMCs. Dispersive Fe-Ti-Si-Cr IMCs caused dispersion strengthening in the Cu weld with large welding heat input. The TC4/304 SS joints fractured in the Ti/weld transition zone.

ACKNOWLEDGMENTS

This study was financially supported by the National Natural Science Foundation of China (Nos. 51674060 and 51605075), the National Key Research and Development Program (No. 2016YFB0701401), the China Postdoctoral Science Foundation (No. 2016M601303), and Guangdong Provincial Key Laboratory of Advanced Welding Technology for Ships (Grant No. 2017B030302010). Also this study was technically supported by the Collaborative Innovation Center of Major Machine Manufacturing in Liaoning.

REFERENCES

1. U. Kamachi, B.M.Ananda. Mudali, K. Rao, R. Shanmugam, and B.Raj. Natarajan: *J. Nucl. Mater.*, 2003, vol. 321, pp. 40–48.
2. E. Norouzi, M. Atapour, and M. Shamanian: *J. Alloy Compd.*, 2017, vol. 701, pp. 335–41.
3. T. Wang, B.G. Zhang, J.C. Feng, and Q. Tang: *Mater. Charact.*, 2012, vol. 73, pp. 104–13.
4. Y. Zhang, D.Q. Sun, X.Y. Gu, and H.M. Li: *Mater. Lett.*, 2016, vol. 185, pp. 152–55.
5. X. Li, J.L. Li, Z.X. Liao, F. Jin, F.S. Zhang, and J.T. Xiong: *Mater. Des.*, 2016, vol. 99, pp. 26–36.
6. H.G. Dong, L.Z. Yu, D.W. Deng, W.L. Zhou, and C. Dong: *J. Mater. Sci. Technol.*, 2015, vol. 31, pp. 962–68.
7. Q.L. Chu, M. Zhang, J.H. Li, and C. Yan: *Mat. Sci. Eng. A.*, 2017, vol. 689, pp. 323–31.
8. M. Gloc, M. Wachowski, T. Plocinski, and K.J. Kurzydowski: *J. Alloy Compd.*, 2016, vol. 671, pp. 446–51.
9. C. Yu, H. Xiao, H. Yu, Z.C. Qi, and C. Xu: *Mat. Sci. Eng. A.*, 2017, vol. 695, pp. 120–25.
10. J.G. Liu, W.C. Cai, L. Liu, J.T. Han, and J. Liu: *Mat. Sci. Eng. A.*, 2017, vol. 703, pp. 386–98.
11. C. Velmurugan, V. Senthilkumar, S. Sarala, and J. Arivarasan: *J. Mater. Process. Tech.*, 2016, vol. 234, pp. 272–79.
12. T.F. Song, X.S. Jiang, Z.Y. Shao, Y.J. Fang, D.F. Mo, D.G. Zhu, and M.H. Zhu: *Vacuum*, 2017, vol. 145, pp. 69–76.
13. H.G. Dong, Z.L. Yang, Z.R. Wang, D.W. Deng, and C. Dong: *J. Mater. Sci. Technol.*, 2015, vol. 31, pp. 217–22.

14. H.G. Dong, Z.L. Yang, G.S. Yang, and C. Dong: *Mat. Sci. Eng. A.*, 2013, vol. 561, pp. 252–58.
15. H.C. Chen, G.J. Bi, Y.B. Lee, and C.K. Cheng: *J. Mater. Process. Tech.*, 2015, vol. 231, pp. 58–65.
16. I. Tomashchuk, P. Sallamand, N. Belyavina, and M. Pilloz: *Mat. Sci. Eng. A.*, 2013, vol. 585, pp. 114–22.
17. S.A.A.A. Mousavi and P.F. Sartangi: *Mat. Sci. Eng. A.*, 2008, vol. 494, pp. 329–36.
18. E. Norouzi, M. Atapour, M. Shamanian, and A. Allafchian: *Mater. Des.*, 2016, vol. 99, pp. 543–51.
19. S. Guo, Q. Zhou, Y. Peng, X.F. Xu, C.L. Diao, J. Kong, T.Y. Luo, K.H. Wang, and J. Zhu: *Mater. Des.*, 2017, vol. 121, pp. 51–60.
20. S.H. Chen, M.X. Zhang, J.H. Huang, C.J. Cui, H. Zhang, and X.K. Zhao: *Mater. Des.*, 2014, vol. 53, pp. 504–11.
21. T. Wang, B.G. Zhang, and J.C. Feng: *Nonferr. Metal. Soc.*, 2014, vol. 2014, pp. 24–14.
22. M. Gao, S.W. Mei, Z.M. Wang, X.Y. Li, and X.Y. Zeng: *Sci. Technol. Weld. Joi.*, 2012, vol. 17, pp. 269–76.
23. I. Tomashchuk, D. Grevey, and P. Sallamand: *Mat. Sci. Eng. A.*, 2015, vol. 622, pp. 37–45.
24. Y. Ustinovshikov, B. Pushkarev, and I. Sapegina: *J. Alloy Compd.*, 2005, vol. 398, pp. 133–38.
25. D.H. Xie, K.Z. Liu, X.B. Xian, L.S. Ye, and Y.P. Chen: *Rare. Metal. Mat. Eng.*, 2008, vol. 37, pp. 1566–69.
26. R.J. Kurtz, M.L. Hamilton, and H. Li: *J. Nucl. Mater.*, 1998, vols. 258–263, pp. 1375–79.
27. T. Wang, B.G. Zhang, G.Q. Chen, and J.C. Feng: *Vacuum*, 2013, vol. 94, pp. 41–47.
28. B.G. Zhang, T. Wang, X.H. Duan, G.Q. Chen, and J.C. Feng: *T. Nonferr. Metal. Soc.*, 2012, vol. 22, pp. 398–403.
29. I. Tomashchuk, P. Sallamand, H. Andrzejewski, and D. Grevey: *Intermetallics*, 2011, vol. 19, pp. 1466–73.
30. J.L. Murray: *J. Phase. Equilib.*, 1983, vol. 4, pp. 81–95.
31. V. Raghavan: *J. Phase. Equilib. Diff.*, 2006, vol. 37, pp. 156–57.
32. Q.L. Chu, R.X. Bai, M. Zhang, J.H. Li, Z.K. Lei, N. Hu, J.M. Bell, and C. Yan: *Mater. Charact.*, 2017, vol. 132, pp. 330–37.
33. Y. Gao, K. Nakata, K. Nagatsuka, F.C. Liu, and J. Liao: *Mater. Des.*, 2015, vol. 65, pp. 17–23.
34. M. Gao, C. Chen, L. Wang, Z.M. Wang, and X.Y. Zeng: *Metall. Mater. Trans. A*, 2015, vol. 46A, pp. 2007–20.
35. A.R. Miedema, P.F.D. Châtel, and F.R.D. Boer: *Physica. B.*, 1980, vol. 100, pp. 1–28.
36. J.A.V. Beek, A.A. Kodentsov, and F.J.J.V. Loo: *J. Alloy Compd.*, 1995, vol. 217, pp. 97–103.
37. K. Liu, Y.J. Li, and J. Wang: *Mater. Manuf. Process.*, 2016, vol. 31, pp. 1–9.
38. MatWeb. <http://www.matweb.com/>. Accessed 22 Jun 2018.